

## Article

# Noncontact and Full-Field Measurement of Residual and Thermal Stress in Film/Substrate Structures

Dong Yang, Xumeng Zhang and Jianguo Zhu \*

Faculty of Civil Engineering and Mechanics, Jiangsu University, Zhenjiang 212013, China; thomas.yd@foxmail.com (D.Y.); 18252111320@163.com (X.Z.)

\* Correspondence: zhujg@ujs.edu.cn

**Abstract:** Residual stress and thermal stress of a film/substrate system are determined based on the curvature measurement with a 3D digital image correlation method (DIC) and calculation of the thin-film stresses by the extension of Stoney's formula. A Ni film electroplated on a H62Cu plate is used to verify the proposed method. The full fields of nonuniform thin-film stresses are obtained in a room temperature to high-temperature environment of 200 °C, which can be potentially extended to higher temperatures. These results provide a fundamental approach to understanding thin-film stresses and a feasible measurement method for high temperature.

**Keywords:** thin film; curvature measurement; stress; digital image correlation method



**Citation:** Yang, D.; Zhang, X.; Zhu, J. Noncontact and Full-Field Measurement of Residual and Thermal Stress in Film/Substrate Structures. *Surfaces* **2021**, *4*, 89–96. <https://doi.org/10.3390/surfaces4010011>

Academic Editor: Gaetano Granozzi

Received: 9 February 2021

Accepted: 3 March 2021

Published: 19 March 2021

**Publisher's Note:** MDPI stays neutral with regard to jurisdictional claims in published maps and institutional affiliations.



**Copyright:** © 2021 by the authors. Licensee MDPI, Basel, Switzerland. This article is an open access article distributed under the terms and conditions of the Creative Commons Attribution (CC BY) license (<https://creativecommons.org/licenses/by/4.0/>).

## 1. Introduction

Thin films are widely used in a large number of technologies ranging from micro-/optoelectronic devices, MEMS/NEMS (thermal sensors and actuators), optical components (lenses, mirrors, filters, etc.) to protective and functional coatings intended to impart thermal, mechanical, tribological, environmental, electrical, magnetic, or biological functions [1]. Thin films can develop large intrinsic stresses during their growth, such as physical or chemical vapor deposition (PVD/CVD), electrochemical deposition, etc., since excessive residual stress levels can dramatically affect the performance, reliability, and durability of thin films as functional components. For example, hard coatings have tensile stress that can lead to cracking and compressive stress can lead to buckling, blistering, and delamination [2]. In addition, stress evolution due to temperature change or thermal cycling is difficult to identify in thin film in electronic packages [3,4] or thermal barrier coatings [5–7]. Various research strategies to tailor and control the stress state are currently being devised, which has generated intense research and innovation activity over the last few decades related to the measurement of stress state in thin films.

A method currently and widely used to estimate the stresses in thin films is based on the measurement of the substrate curvature. As a pioneering work, Stoney derived a relationship between the film stress and the amount of substrate bend in the early 1900s [8]. Because it is nondestructive and can be used in real-time, it has been widely used for quantifying stress in thin films [9–11]. However, the rigid assumptions of Stoney's formula, such as uniform thin-film stress, uniform deformation over the entire system, and infinitesimal strains and rotations of the system, cannot be satisfied in real situations [12]. Feng et al. derived an extension of Stoney's formula for a multilayer thin-film/substrate system subjected to nonuniform and nonaxisymmetrical temperature distribution [13,14]. As for the curvature measurement, multiple techniques have been developed, such as laser scanning, shearing interferometry [15,16], coherent gradient sensing [17,18], multi-beam optical stress sensor [19], and so on. The 3D digital image correlation (DIC) method is a full-field, real-time, noncontact optical technique which is insensitive to vibration and able to provide the full-field curvatures of specimens [20]. Moreover, out-of-plane displacement and curvature can be automatically obtained without phase analysis of

interference fringes. This work presents an effective method based on 3D DIC for full-field slopes and curvature measurement of a Ni/Cu film in a high-temperature environment going from room temperature to 200 °C. Nonuniform residual stress and thermal stress of the thin film at high temperature are obtained by the extension of Stoney’s formula. The stress evolution process of the film was analyzed.

### 2. Theoretical Equation

A thin film deposited on a circular substrate of radius R is shown in Figure 1. The film and substrate were subjected to uniform temperature distribution. The film is modeled as a membrane since it is very thin ( $h_f$ ) and the substrate is modeled as a plate of small thickness ( $h_s$ ). The radial and circumferential stresses of the thin film can be obtained from the linear thermoelastic constitutive model, and the theoretical relationship between the curvature of the sample of the disk thin film and the stress of the thin film can be obtained through formula derivation [13,14]:

$$\sigma_{rr}^f - \sigma_{\theta\theta}^f = \frac{E_s h_s^2 \alpha_s}{6(1 - \nu_s)} \frac{E_f}{1 + \nu_f} \frac{k_{rr} - k_{\theta\theta}}{A_{\nu\alpha}} \tag{1}$$

$$\sigma_{rr}^f + \sigma_{\theta\theta}^f = \frac{E_s h_s^2}{6(1 - \nu_s)} \frac{E_f}{1 - \nu_f} \left[ \frac{\alpha_s - \alpha_f}{A_\alpha} \overline{k_{rr} + k_{\theta\theta}} + \frac{(1 + \nu_s)\alpha_s - 2\alpha_f}{(1 + \nu_s)A_{\nu\alpha}} (k_{rr} + k_{\theta\theta} - \overline{k_{rr} + k_{\theta\theta}}) \right] \tag{2}$$

where  $A_\alpha \equiv \frac{E_f h_f}{1 - \nu_f} (\alpha_s - \alpha_f)$ ,  $A_{\nu\alpha} = \frac{E_f h_f}{1 - \nu_f^2} [(1 + \nu_s)\alpha_s - (1 + \nu_f)\alpha_f]$  are constant;  $k_{rr} = \frac{d^2 w}{dr^2}$  is the radial curvature,  $k_{\theta\theta} = \frac{1}{r} \frac{dw}{dr}$  is the circumferential curvature;  $\overline{k_{rr} + k_{\theta\theta}} = \frac{1}{\pi R^2} \iint_A (k_{rr} + k_{\theta\theta}) \eta d\eta d\theta = \frac{2}{R^2} \int_0^R \eta (k_{rr} + k_{\theta\theta}) d\eta$  is the average system curvature. The Young’s modulus, Poisson’s ratio, and coefficient of thermal expansion are denoted by  $E_f, E_s; \nu_f, \nu_s;$  and  $\alpha_f$  and  $\alpha_s$ , respectively, and the subscripts “f” and “s” denote the thin film and substrate, respectively.  $w$  is displacement along the  $z$  direction. The interface shear stress can also be directly related to the system curvature:

$$\tau = \frac{E_s h_s^2}{6(1 - \nu_s^2)} \frac{d(k_{rr} + k_{\theta\theta})}{dr}. \tag{3}$$

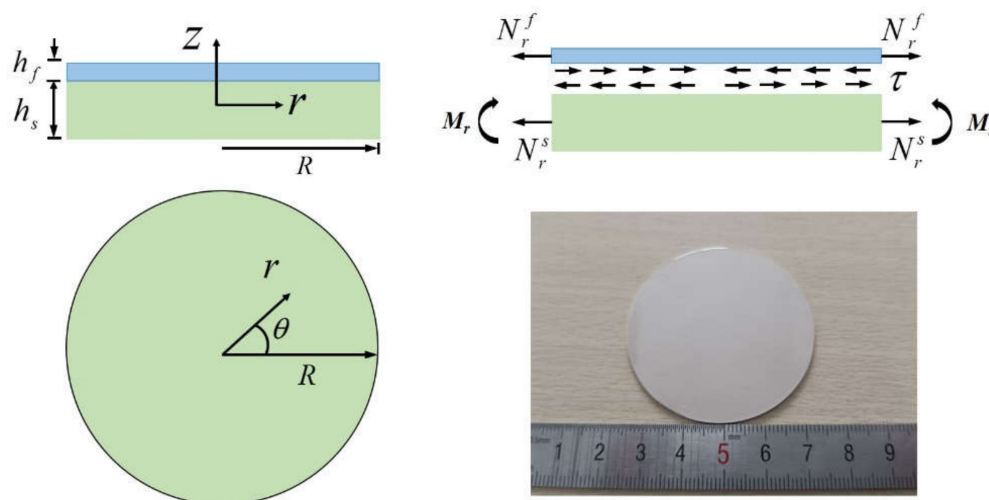
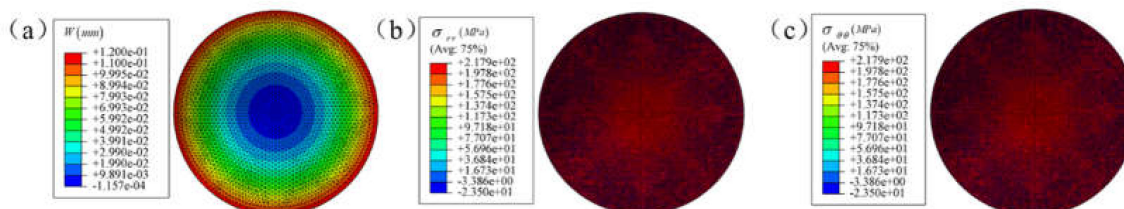


Figure 1. Schematic and photo of a thin-film/substrate system.

### 3. Numerical Simulation

A 3D finite element model of film/substrate system was established as shown in Figure 2a, in which the thin film was Ni and the substrate was H62Cu. The mechanical properties are shown in Table 1. The sample was isothermally heated from room temperature (25 °C) to 140 °C with a free boundary condition, and the radial and circumferential stresses of the film were calculated. Linear elasticity was assumed for all the materials.



**Figure 2.** Numerical simulation results: (a) off-plane deformation field; (b) radial stress field of the film; (c) the circumferential stress field of the thin film.

**Table 1.** Dimension and physical properties of specimen [21,22].

	Diameter (mm)	Thickness ( $\mu\text{m}$ )	$E$ (GPa)	$\nu$	$\alpha$ ( $\times 10^{-6}/^{\circ}\text{C}$ )
Substrate(H62Cu)	50	500	100	0.324	18.8
Film(Ni)	50	10	207	0.291	13

The results indicate that the simulated radial and circumferential stresses of the film are equal, as shown in Figure 2b,c. The full-field curvature of the sample was obtained based on the deformation field in Figure 2a. Then, the full-field curvature was substituted into the extended Stoney formula to calculate the film stress, as shown in Figure 3. It is found that the error of the film stress calculated by the formula is 1.9%, which is a small error. The formula and calculation method of thin film stress have been verified.

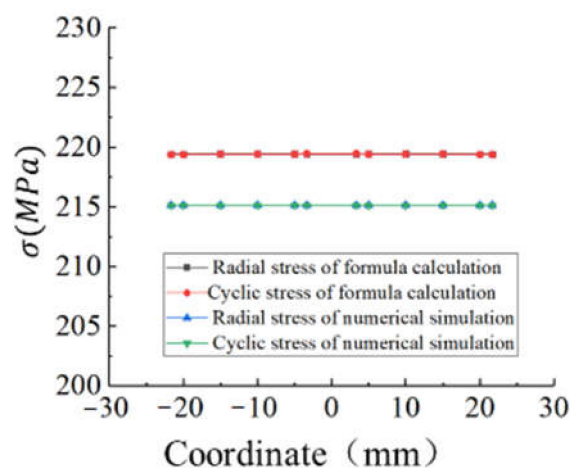


**Figure 3.** The simulation results and the theoretical calculation of stress with position.

### 4. Experiment

The schematic of experimental setup is shown in Figure 4. A 3D digital image correlation system [23] was used a noncontact, non-interferometric, image-based optical technique for whole-field deformation measurement. VIC-3D is a simple optical method to measure the deformation of the surface of an object. The method directly uses the gray changes of two digital images before and after the surface deformation to measure the surface displacement and deformation field of the object. Details are shown in reference [23]. The system

was equipped with two CCD cameras (Schneider 2.8/50-0902, Fronhausen, Germany) with a resolution of  $1624 \times 1224$  pixels<sup>2</sup>. The focusing length of the camera is 50 cm. The distance between the sample and camera is 49.6 cm. The depth of focus is 39.3 cm. The incident angle of the light axis of the camera to the sample surface was  $22.5^\circ$ . The light sources were two identical white light sources. Note that it is not necessary to use two white light sources. However, the use of two light sources can make the illumination uniform with better image quality and allow obtaining more accurate calculation results. A H62 brass plate, electroplated with nickel on one side, was used as specimen, as shown in Figure 1. This size sample is only to verify the feasibility of the thin film stress measurement method. An electrical heating chamber was used to heat the specimen from room temperature to  $200^\circ\text{C}$  and the temperature was measured and controlled with a temperature controller. When the intended temperature was achieved, the sample surface image was captured for subsequent DIC analysis (Vic-3D, Correlated Solutions, Inc., Keasbey, NJ, USA). It should be noted that an artificial speckle pattern was made on the test specimen surface as a carrier of deformation information. The dimension and physical properties of the specimen are listed in Table 1.

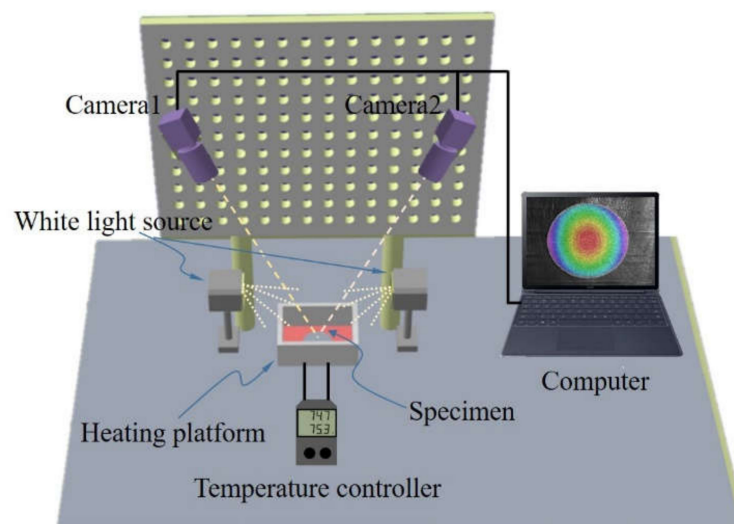


**Figure 4.** Schematic of the experimental setup.

Residual and thermal stress measurement of the thin film structure by DIC method uses the following procedures. Firstly, the two-camera 3D DIC system was calibrated by acquiring image pairs of a standard grid undergoing arbitrary motions. The calibration plate had specially marked points with known spatial position and no collinearity. Moving the calibration plate, the images of the calibration plate with different positions were obtained by CCD camera. The images were imported into the VIC program to calculate the three-dimensional spatial coordinate system. The calibrated image was  $47.44 \mu\text{m}/\text{pixels}$ , and the theoretical accuracy of deformation measurement was  $0.47 \mu\text{m}$  based on the DIC optimal match confidence of 0.01 pixels [23]. According to the sample size  $r = 25 \text{ mm}$ , the curvature measurement error is  $1.5 \times 10^{-6} \text{ mm}^{-1}$ , and the calculated stress error is  $0.92 \text{ MPa}$ . Second, the specimen was horizontally placed on the heating chamber without any restraint. The white light sources were turned on to illuminate the sample surface during the experiment. Then, the sample surface before and after electroplating was captured for subsequent residual stress measurement. In addition, the sample surface at  $80$ ,  $140$ , and  $200^\circ\text{C}$  was captured for subsequent thermal stress measurement. Finally, these images were analyzed by the DIC technique to extract out-of-plane displacements and corresponding curvatures. A subset of  $40 \times 40$  pixels<sup>2</sup> and a step size of 10 pixels were selected in the calculation.

## 5. Results and Discussion

### 5.1. Residual Stress

Morphology diagrams of substrate before electroplating and after electroplating at room temperature are shown in Figure 5a,b. The corresponding out-of-plane deformation diagram of the thin structure based on 3D DIC calculation is shown in Figure 5c, which will be used for determination of residual stress because of the electroplating process.  $z$  is the coordinate height, and  $w$  is the relative displacement in the height direction. It should be noted that the substrate has a very small curvature (order of  $10^{-4} \text{ mm}^{-1}$ ) before electroplating due to the machining process and is approximately regarded as a plate. Similarly, Figure 5b was set as reference image, and morphology diagrams of the electroplating sample at 80, 140, and 200 °C were set as deformed images (not shown), then the out-of-plane deformation diagrams of the thin structure were calculated and are shown in Figure 5d–f, which will be used for determination of thermal stress due to temperature variation. The off-plane displacement refers to the displacement of the morphology at room temperature in the direction of height.

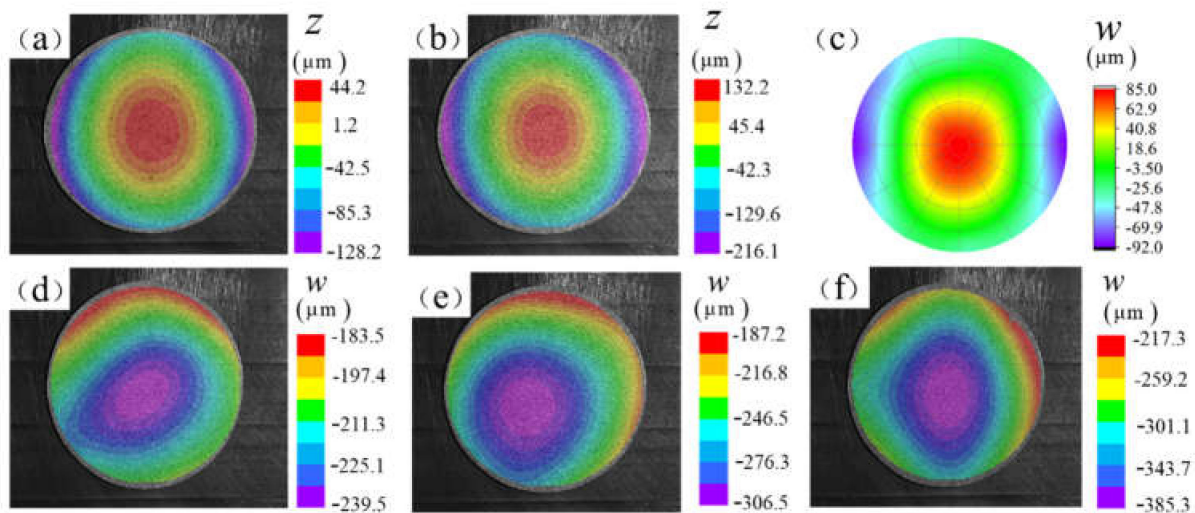


**Figure 5.** Morphology diagram of sample: (a) before electroplating and (b) after electroplating at room temperature. Out-of-plane deformation diagram of the electroplating sample at: (c) the substrate is electroplated, (d) 80 °C, (e) 140 °C, and (f) 200 °C.

To calculate the residual stress due to the electroplating process, Zernike polynomials were used to fit the out-of-plane displacement map (Figure 5c) and differentiated to extract the radial and circumferential curvatures of the thin structure according to Equations (1)–(3). As shown in Figure 6, the curvature fields of the electroplating sample show nonuniform distribution and the curvatures in the vicinity of the edge become obviously much greater than those in the other area due to the edge effect. Then, the distribution of residual stress in the electroplating film is calculated as shown in Figure 6. It can be observed that the radial and circumferential stresses of the thin film are compressive stress; the averaged magnitude of the radial and circumferential stresses of the thin film is  $-215.7$  and  $-217.4$  MPa, respectively. In addition, the interface shear stress is relatively small with maximum value less than 0.1 MPa. The residual stress caused by electroplating is related to electroplating material, substrate thickness, electroplating environment, and electroplating thickness.

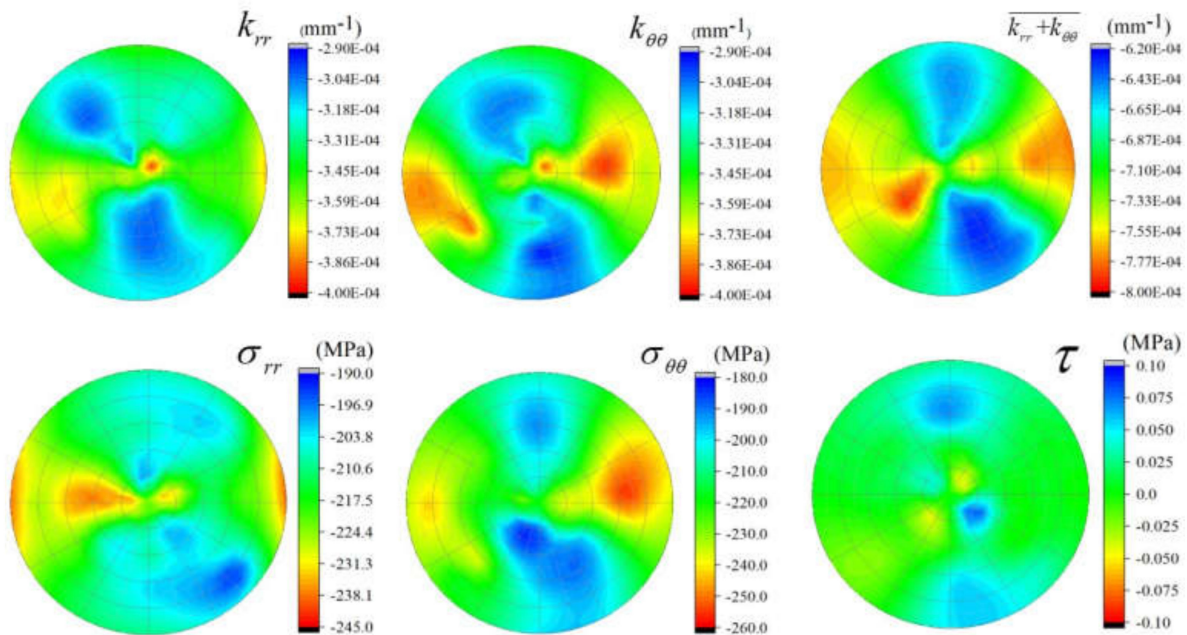


**Figure 6.** Distribution of curvature and residual stress of the electroplating film.

The radial residual stress and circumferential residual stress produced by electroplating are compressive stress, mainly because the coefficient of thermal expansion of substrate is greater than that of nickel film. After electroplating at 70 °C, the sample is placed at room temperature, and the brass substrate has a greater shrinkage than the nickel film, so the substrate produces compressive stress on the film. In reference [8], the residual stress generated in the Ni/Cu system is compressive stress, and the value is close to this experiment. In reference [12], the residual stress generated in the SiO<sub>2</sub>/Si system is also compressive stress.

### 5.2. Thermal Stress

Firstly, when the intended temperature was achieved, the sample surface image was captured for subsequent DIC analysis to obtain the deformation field. Secondly, the thermal deformation field was substituted into the self-written program to obtain the discrete curvature field and the discrete curvature component was then substituted into the extended Stoney formula to calculate the radial and circumferential thermal stress fields. The distribution of radial and circumferential thermal stresses of the electroplating film at 80, 140, and 200 °C are shown in Figure 7. It can be observed that the radial and circumferential thermal stresses of the electroplating film change to tensile stress at elevated temperatures. The averaged radial thermal stress of the electroplating film at 80, 140, and 200 °C is 107.8, 223.3, and 312.8 MPa, respectively, and the averaged circumferential thermal stress is 105.6, 225.9, and 314.6 MPa, respectively. Obviously, the averaged value of radial thermal stress and circumferential thermal stress is close to each other and is getting larger with the increasing temperature. Moreover, the full field of the nonuniform distribution of the thin-film stress is obtained with the elevated temperature. When measuring the thermal stress of the film in isothermal state, the values of the radial and circumferential stresses of the film are equal. However, in the experiment, since the thickness of the film and substrate were not strictly uniform, the heating temperature field was not strictly an isothermal environment. Hence, the curvature field measured in the experiment is not uniform, as a result, the calculated radial and circumferential thermal stress distribution is not uniform. The film stress is obtained by superposition of residual stress and thermal stress in the film.

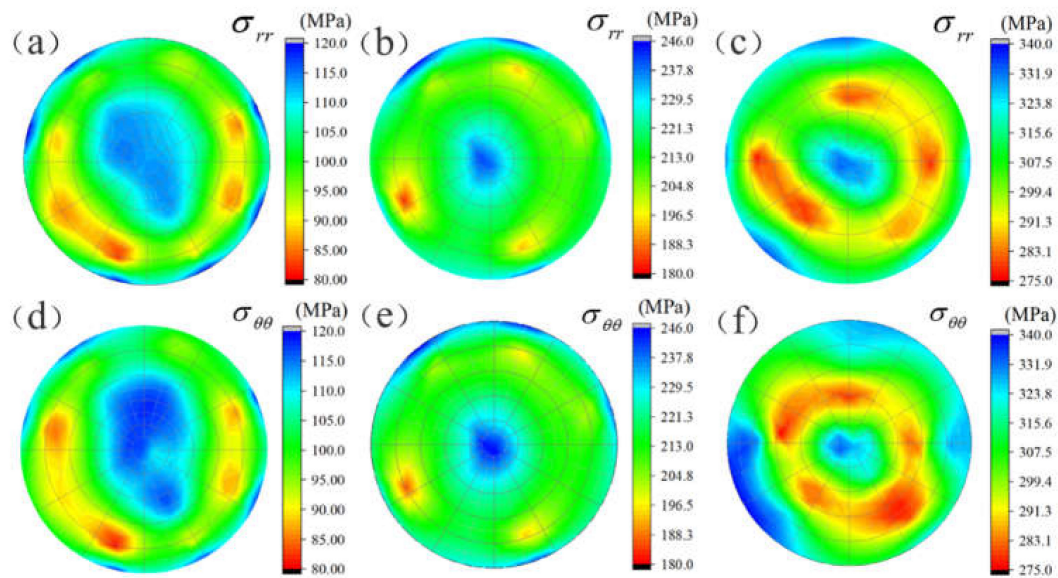


**Figure 7.** Distribution of radial and circumferential thermal stress of the electroplating film at 80 °C (a,d), 140 °C (b,e), and 200 °C (c,f).

## 6. Conclusions

The results presented here demonstrate the use of a 3D digital image correlation method to measure the thin-film/substrate system curvature at high temperature and calculate the nonuniform stresses of the film by the extension of Stoney's formula. This optical technique is featured as full-field nonuniform curvature measurement. A Ni film electroplated on a H62Cu plate is used to verify the proposed method. These results provide a fundamental approach to understand thin-film stresses and a feasible measurement method for residual stress and thermal stress.

**Author Contributions:** Experiment, D.Y.; data curation, D.Y.; validation, X.Z.; writing—original draft preparation, D.Y.; writing—review and editing, J.Z. All authors have read and agreed to the published version of the manuscript.

**Funding:** This research received no external funding.

**Institutional Review Board Statement:** Not applicable.

**Informed Consent Statement:** Not applicable.

**Data Availability Statement:** Data is contained within the article.

**Conflicts of Interest:** The authors declare no conflict of interest.

## References

1. Abadias, G.; Chason, E.; Keckes, J.; Sebastiani, M.; Thompson, G.B.; Barthel, E.; Doll, G.; Murray, C.; Stoessel, C.H.; Martinu, L. Review Article: Stress in thin films and coatings: Current status, challenges, and prospects. *J. Vac. Sci. Technol. A* **2018**, *36*, 020801. [[CrossRef](#)]
2. Chason, E.; Guduru, P.R. Tutorial: Understanding residual stress in polycrystalline thin films through real-time measurements and physical models. *J. Appl. Phys.* **2016**, *119*, 1032–1114. [[CrossRef](#)]
3. Yamamoto, T.; Nagayama, T.; Nakamura, T. Thermal Expansion and Thermal Stress Behavior of Electroless-Plated Fe–Ni–B Alloy Thin Film for High-Density Packaging. *J. Electrochem. Soc.* **2018**, *166*, D3238–D3245. [[CrossRef](#)]
4. Zhang, X.; Meng, H.; Wang, H.; Guo, F. Effect of thermal misfit stress on steam-driven delamination in electronic packages. *Eng. Fract. Mech.* **2018**, *194*, 61–72. [[CrossRef](#)]
5. Zhu, J.G.; Xie, H.M.; Li, Y.J.; Hu, Z.X.; Luo, Q.; Gu, C.Z. Interfacial Residual Stress Analysis of Thermal Spray Coatings by Miniature Ring-Core Cutting Combined with DIC Method. *Exp. Mech.* **2014**, *54*, 127–136. [[CrossRef](#)]
6. Yang, X.; Liu, Z.; Xie, H. A real time deformation evaluation method for surface and interface of thermal barrier coatings during 1100 °C thermal shock. *Meas. Sci. Technol.* **2012**, *23*, 105604. [[CrossRef](#)]

7. Zhu, J.G.; Chen, W.; Xie, H.M. Simulation of residual stresses and their effects on thermal barrier coating systems using finite element method. *Sci. China Phys. Mech. Astron.* **2015**, *58*, 1–10. [[CrossRef](#)]
8. Stoney, G. The tension of metallic films deposited by electrolysis. *J. R. Soc. Lond. Ser. A* **1909**, *82*, 172–175.
9. Yu, H.Z.; Thompson, C.V. Effects of oblique-angle deposition on intrinsic stress evolution during polycrystalline film growth. *Acta Mater.* **2014**, *77*, 284–293. [[CrossRef](#)]
10. Yu, H.Z.; Thompson, C.V. Grain growth and complex stress evolution during Volmer–Weber growth of polycrystalline thin films. *Acta Mater.* **2014**, *67*, 189–198. [[CrossRef](#)]
11. Al-Masha'Al, A.; Bunting, A.; Cheung, R. Evaluation of residual stress in sputtered tantalum thin-film. *Appl. Surf. Sci.* **2016**, *371*, 571–575. [[CrossRef](#)]
12. Dong, X.; Feng, X.; Hwang, K.-C.; Ma, S.; Ma, Q. Full-field measurement of nonuniform stresses of thin films at high temperature. *Opt. Express* **2011**, *19*, 13201–13208. [[CrossRef](#)] [[PubMed](#)]
13. Dong, X.L.; Feng, X.; Hwang, K.C. Non-uniform stress distribution and deformation bifurcation of thin film/substrate system subjected to gradient temperature. *Thin Solid Films* **2011**, *519*, 2464–2469. [[CrossRef](#)]
14. Feng, X.; Huang, Y.; Rosakis, A.J. Stresses in a Multilayer Thin Film/Substrate System Subjected to Nonuniform Temperature. *J. Appl. Mech.* **2008**, *75*, 021022. [[CrossRef](#)]
15. Zhang, C.; Dong, X.; Feng, X.; Hwang, K.-C. Multiwavelength shearing interferometry for measuring the slopes, curvatures, and shapes of thin films/substrate systems. *Opt. Lett.* **2013**, *38*, 5446–5449. [[CrossRef](#)] [[PubMed](#)]
16. Tippur, H.V. Simultaneous and real-time measurement of slope and curvature fringes in thin structures using shearing interferometry. *Opt. Eng.* **2004**, *43*, 3014–3020. [[CrossRef](#)]
17. Ma, K.; Xie, H.; Zhu, J. Two modified coherent gradient sensing methods for slope measurement of reflective surfaces. *Meas. Sci. Technol.* **2014**, *25*, 125202. [[CrossRef](#)]
18. Dong, X.; Zhang, C.; Feng, X.; Duan, Z. Analysis and improvement of accuracy, sensitivity, and resolution of the coherent gradient sensing method. *Appl. Opt.* **2016**, *55*, 4752–4758. [[CrossRef](#)]
19. Colin, J.J.; Abadias, G.; Michel, A.; Jaouen, C. On the origin of the metastable beta-Ta phase stabilization in tantalum sputtered thin films. *Acta Mater.* **2017**, *126*, 481–493. [[CrossRef](#)]
20. Pan, B. Digital image correlation for surface deformation measurement: Historical developments, recent advances and future goals. *Meas. Sci. Technol.* **2018**, *29*, 082001. [[CrossRef](#)]
21. Pelleg, J. Mechanical properties of materials. *Solid Mech. Appl.* **2013**, *190*, 1–634.
22. Touloukian, Y.S.; Kirby, R.K.; Taylor, R.E.; Desai, P.D. *Thermophysical Properties of Matters. Thermal Expansion of Metallic Elements and Alloys*; Plenum: New York, NY, USA, 1976; Volume 12.
23. Sutton, M.A.; Orteu, J.J.; Schreier, H. *Image Correlation for Shape, Motion and Deformation Measurements*; Springer: New York, NY, USA, 2009.